

Effect of Second-Stage-Aging on the Fatigue Properties of Maraging Steel

Norio Kawagoishi¹, Kohji Kariya¹, Takanori Nagano², Yuzo Nakamura³

¹ Department of Mechanical System Engineering, Daiichi Institute of Technology
Kirishima 899-4395, Japan

² Department of Mechanical Engineering, Miyakonojo National College of Technology
Miyakonojo 885-8567, Japan

³ Department of Mechanical Engineering, Graduate School of Science and Engineering
Kagoshima University, Kagoshima 890-0065, Japan

* Corresponding author: nakamura@mech.kagoshima-u.ac.jp

Abstract Maraging steels are known to have not only ultrahigh strength but also large toughness so that they are promised to be as used as components or parts with structural integrity. It is also known that maraging steels are conventionally aged in two steps to obtain such good mechanical properties. Some of the present authors showed that one-step-aged maraging steels exhibited the increase in fatigue strength at intermediately high temperatures of 473 K and 673 K, compared with the strength obtained at room temperature. In addition, when low-temperature aging at 473 K and 673 K was given to one-step-aged maraging steels by varying the aging time, this second-step-aging increased the hardness of the steel. It also increased fatigue strength in an environmental situation where high humidity markedly reduced the fatigue life of one-step-aged steels. These results strongly suggest that the second-step-aging at low temperatures produces some additional microstructures which impede plastic deformation and increases resistance to fatigue cracking, even in the environmental conditions which accelerate the deformation and fracture. In the present report, a microstructural model will be proposed to interpret the effect of second-step-aging on the mechanical properties of maraging steel, which will explain the improvement of fatigue strength at intermediately high temperature and in high humidity condition.

Keywords Maraging steel, Fatigue, Two-step-aging, Microstructure, Environmental effect

1. Introduction

The high strength of maraging steels is principally based on the strengthening due to the martensitic transformation of Fe-18mass%Ni alloy, which also accompanies the introduction of dislocations with high density [1, 2]. According to a recent study of Nakashima *et al.* [3], the dislocation density introduced by martensitic transformation becomes $7 \times 10^{15} / \text{m}^2$ in ultra-low carbon Fe-18mass%Ni (0.002mass%C), leading to the yield strength of 0.66 GPa. The addition of alloying element such as Mo, Ti and Co increases the strength of maraging steels substantially by the precipitation hardening obtained by aging [1, 2]. As a result, the maraging steels exhibit the ultrahigh strength up to more than 2 GPa, without losing ductility and fracture toughness significantly. These mechanical properties are beneficial from the viewpoints of the structural integrity and the reduction in weight in practical applications.

The high strength and large ductility generally improve the fatigue strength. However it is well known that the fatigue properties of steels are very sensitive to environment [4]. Exposure to humid air or to aqueous solutions leads to the prominent deterioration of fatigue strength in high strength steels like maraging steel. Our previous studies [5–7] showed that the fatigue strength of 18Ni maraging steels aged at 753 K was lowered markedly by exposing the steel to humid air with a relative humidity (RH) of 85%. The susceptibility of fatigue strength to humidity increases with aging time in one-step-aged maraging steel, which leads to the lowest fatigue strength at peak-aging [6, 7]. The application of the second-step-aging at 673 K to the one-step-aged steel, however,

recovered the susceptibility comparable to the under-aged states. In another previous study [8], the fatigue strength of a 300G maraging steel under-aged at 753 K was shown to increase at test temperatures of 473 K and 673 K. It was also demonstrated that the hardness increases with the number of cycles at these temperatures. The second-stage-aging of this type is, hence, very effective to improve the fatigue properties at moderately elevated temperatures.

The results in the previous studies mentioned above suggest that microstructural change is induced by the static second-step-aging to improve the fatigue strength in humid air, and that dynamical aging is also caused during deformation at moderately elevated temperatures. In addition, these effects appear prominently in fatigue properties. In the present study, we try to understand the effects of the second-step-aging on the fatigue properties of maraging steels from the microstructural aspect. For this purpose, we reassess the results of previous studies. In particular, we investigate the dependence of hardness change on aging time and temperature in detail, taking into account the microstructural analyses by means of transmission electron microscopy (TEM). Based on these reassessment and analyses, the strengthening mechanism due to the second-step-aging and its role in suppressing the deterioration of fatigue properties will be discussed.

2. Experimental procedures

Chemical compositions of 300G and 350G maraging steels used are shown in Table 1. Both steels were supplied as rods of 13 mm diameter, and experienced the solution treatment conducted at 1123 K for 5.4 ks. The 300G steel was aged at 753 K for 48 ks, which led to an under-aged state. For the 350G steel, two under-aged conditions were obtained at 753 K by using the aging times of 11 ks and 100 ks, while the peak-aging was attained by heating the specimen at 753 K for 150 ks. The 300G steel specimens were subjected to rotating bend test with a frequency of 50 Hz at room temperature, 473 K and 673 K, to examine the effect of test temperature on the fatigue properties. For the 350G steel, the peak-aged specimens were subjected to second-step-aging at 473 K and 673 K by changing the keeping time, prior to tensile and rotating bend tests at room temperature. The fatigue tests of the 350G steel specimens were carried out in air with the RH of 25% and 85% to examine the influence of humidity on the fatigue properties. The details of experimental procedures used for the above fatigue tests had been reported in the previous papers [5–8]. Hereafter we assign S and D to the one-step-aging and two-step-aging, and U, P and O to the under-, peak- and over-aging, respectively, as will be shown in Table 2.

The second-stage-aging at 473 K and 673 for various time up to 800 ks was applied to the under-aged 300G steel and the peak-aged 350G steel. The Vickers hardness of the polished surfaces of these specimens was measured by using a load of 9.8 N to examine the change in hardness during the second-step-aging. The microstructures of one-step-aged and two-step-aged 350G specimens were also observed by TEM. In addition, an electrolyte extraction technique was used to identify the precipitates and evaluate their contents.

Table 1. Chemical compositions of maraging steels (mass%).

| Grade | Ni | Mo | Co | Ti | Al | Mn | Si | S | C | Fe |
|-------|-------|------|-------|------|------|------|------|-------|-------|------|
| 300G | 18.4 | 5.14 | 9.09 | 0.89 | 0.11 | 0.01 | 0.05 | 0.002 | 0.005 | bal. |
| 350G | 17.89 | 4.27 | 12.36 | 1.3 | 0.08 | 0.01 | 0.01 | | 0.001 | bal. |

3. Results

3.1 Relation between the tensile properties and hardness

Table 2 shows the yield strength (σ_y) given by 0.2% proof stress, the tensile strength (σ_{max}), the

reduction of area and the Vickers hardness (H_V) obtained for age-hardened 300G and 350G maraging steels. The aging conditions are also listed in this table. One can see from this table that under-aged 300G steel (SA-U0) has the lowest strength and hardness. It also exhibits the smallest reduction of area which represents the ductility. The increase of keeping time in one-step-aging heightens the static strength of 350G steel to the peak strength obtained at 150 ks. However, when the aging-time is longer than this, softening appears. This result suggests that over-aging is induced by the coarsening of precipitates. Fig. 2 shows the relation of the yield strength and tensile strength with the Vickers hardness. It is well known that the strength measured by tensile tests has a linear relationship with the Vickers hardness, *i.e.*, $\sigma = CH_V$, where C is a numerical constant and generally about 1/3 [9, 10]. As can be seen from solid lines depicted in Fig. 2, this relation is satisfied in the one-step-aged specimens and the value of C becomes 0.334 for yield strength and 0.346 for tensile strength. However the two-step-aged specimens do not exhibit such linear relations in both of the yield and tensile strengths. It has not been clarified why this phenomenon occurs, but the change in hardness seems to be more sensitive to microstructural change than the macroscopic properties obtained by tensile tests.

Table 2 shows the tensile properties and Vickers hardness of 300- and 350G steels

| Grade | Aging condition (specification) | Yield strength, σ_y (GPa) | Tensile strength, σ_{max} (GPa) | Reduction of area (%) | Vickers hardness, H_V (GPa) |
|-------|---------------------------------|----------------------------------|--|-----------------------|-------------------------------|
| 300 | 753 K, 48 ks (SA-U0) | 2.07 | 2.16 | 47 | 6.21 |
| 350 | 753 K, 11 ks (SA-U1) | 2.19 | 2.23 | 54 | 6.52 |
| | 753 K, 100 ks (SA-U2) | 2.27 | 2.31 | 54 | 6.76 |
| | 753 K, 150 ks (SA-P) | 2.30 | 2.44 | 54 | 6.91 |
| | SA-P + 673 K, 72 ks (DA-U) | 2.33 | 2.42 | 52 | 7.35 |
| | SA-P + 673 K, 400 ks (DA-P) | 2.42 | 2.55 | 51 | 7.69 |
| | SA-P + 673 K, 673 ks (DA-O) | 2.34 | 2.44 | 55 | 7.35 |

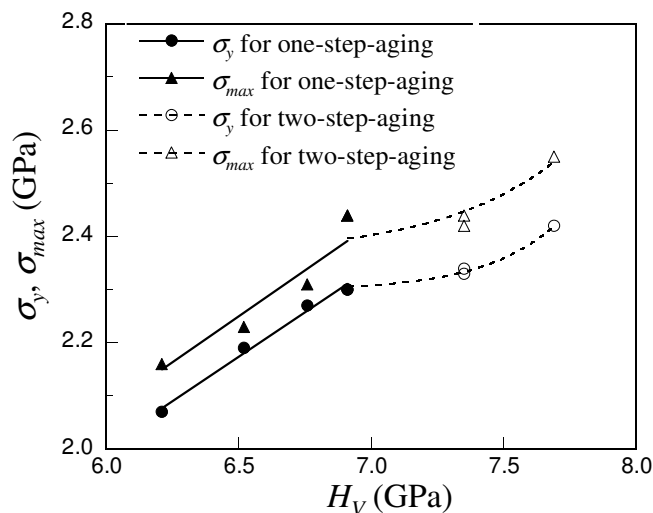


Fig. 2. The relation of yield and tensile strengths with hardness.

3.2 Change in hardness during second-step-aging

Fig. 3 shows the change in hardness with the time of second-step-aging at 473 K and 673 K, which is obtained for SA-P and SA-U0 specimens. The hardness increases very slowly at short time and then rapidly at longer time. SA-P specimen aged at 673 K, however, shows the saturation of hardness increase at 400 ks and the softening due to over-aging at longer time. Instead, the increase

in hardness due to the second-step-aging is retarded in SA-P specimen aged at 473 K, and the saturation of hardness does not appear during the time investigated. The same trend can be seen in SA-U0 specimens aged at 473 K and 673 K, while the increase in hardness occurs earlier than SA-P specimens.

The increase in hardness, ΔH_V , during the second-step-aging is considered to arise from the formation of atmosphere of solute atoms or precipitates due to this aging, as will be mentioned later. It is well known that the evolution of precipitates frequently obeys the Johnson-Mehl-Avrami equation in which the volume fraction of precipitates can be written as [11]

$$f = f_o \{1 - \exp(-kt^n)\}, \quad (1)$$

where f_o is the saturation value of volume fraction, t is time, and k and n are constants. It is believed that the hardening during the second-step-aging till the peak-hardening is caused by the shear-cutting of the newly formed precipitates by mobile dislocations. Thus the increase in hardness may be given by $\Delta H_V = Ar^{1/2}f^{1/2}$, where A is a constant and r is the radius of particles, according to the theory of precipitation hardening [12]. As will be discussed later, the coefficients of lattice diffusion of substitutional solute atoms are too small to contribute to the precipitation at 473 K. Instead their diffusion along dislocations (pipe diffusion) is considered to play a major role in the precipitation at such low temperatures. In this case the particle size is given by [13]

$$r = B\{D_d(RT)\}^{1/5}t^{1/5}, \quad (2)$$

where B is a constant, D_d is the coefficient of pipe diffusion, R is the gas constant and T is the absolute temperature. Taking into account the incubation time t_i , which appears as the retardation of the hardness increase at 473K, we can obtain the following formula for the increase in hardness.

$$\Delta H_V = \beta(t - t_i)^{1/10} \{1 - \exp[-k(t - t_i)^n]\}^{1/2}, \quad (3)$$

where $\beta = ABf_o\{D_d(RT)\}^{1/10}$. This equation reproduces the measured values of ΔH_V fairly well in each specimen and for each second-step-aging condition, as is shown by solid curves in Fig. 3.

Table 3 shows the values of parameters in Eq. (3). The values of β and n at 473 K are nearly equal in SA-U0 and SA-P specimens, which suggests that the precipitation proceeds with the same

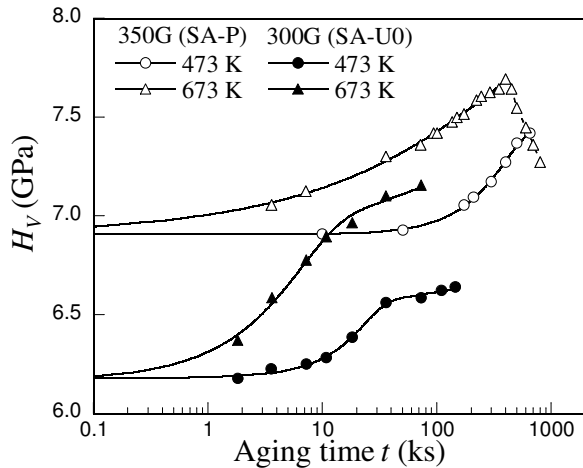


Fig. 3. Change of hardness with time during second-step-aging.

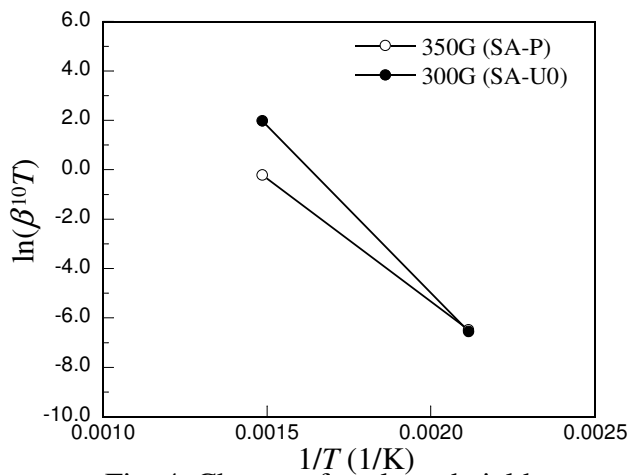


Fig. 4. Change of evaluated yield strength with aging time.

Table 3. The values of parameters in equation (4) and the activation energy of diffusion.

| Specimen | T (K) | β (GPa/ks ^{1/10}) | n | k (/ks ^{n}) | t_i (ks) | Q_d (kJ/mol) |
|-----------------|---------|-----------------------------------|------|--------------------------------------|------------|----------------|
| 300G (SA-U0) | 473 | 0.281 | 2.35 | 4.63×10^{-4} | ~0 | 113 |
| | 673 | 0.636 | 1.44 | 0.0531 | 0.02 | |
| 350G (SA-P) | 473 | 0.283 | 2.34 | 4.37×10^{-7} | 6.47 | 82.9 |
| | 673 | 0.511 | 0.54 | 0.0377 | 0.01 | |

mechanism in both specimens. This trend can be seen at 673 K. However, since the value of n indicates the morphology of precipitates or the precipitation process [11], the smaller values of n at 673 K suggest that the nature of precipitates at this temperature may differ from that of 473 K. It should be also noted that the evaluated incubation time is very small except SA-P specimen aged at 673 K, suggesting that the precipitation starts very quickly. The assumed activation energy of pipe diffusion, Q_d , can be evaluated from the values of $\beta^{10}T$. Fig. 4 shows the Arrhenius plots of $\beta^{10}T$ evaluated for SA-P and SA-U0 specimens. The slopes of straight lines in this figure yield 82.9 kJ/mol and 113 kJ/mol for the value of Q_d in SA-P and SP-U specimens, respectively (Table 3). These values of Q_d are nearly one third or half of the activation energy of lattice diffusion, Q_l (for instance, $Q_l = 244$ kJ/mol for Ni in pure Fe), and close to the activation energy of dynamic strain aging in Fe-Ni alloys (~110 kJ/mol) and Fe-Si alloy (125 kJ/mol) measured by Cuddy and Leslie [14]. Cuddy and Leslie suggest that the pipe diffusion of substitutional solute atoms which have large solution-hardening effects contributes to the occurrence of dynamic strain aging, since C atoms in the alloys they used are believed to be removed by the addition of Ti. The contribution of C atoms is also believed to be negligibly small in the maraging steels investigated here, because the content of C atoms is too small to yield the observed increase of hardness and the diffusion coefficients of C atoms at 473 K and 673 K are too large to explain the very slow increase of hardness at these temperatures.

3.3 Dynamic aging during fatigue tests

Fig. 5 shows the SN curves of SA-U0 specimen tested at room temperature, 473 K and 673 K. The increase in test temperature markedly increases the fatigue strength in high cycle fatigue region, and the increase of fatigue strength at the number of cycles larger than about 5×10^5 seems to be larger at 673 K than at 473 K. These results are in contrary with the fact that the yield strength decreases as the test temperature is increased [5]. In order to reassess the previous data, we use the following formula for the relation of stress amplitude (σ_a) with the number of cycles (N_f).

$$\sigma_a = \sigma_{ao} + k\{(N_f/N_{fo})^{-a} - 1\}^b \quad (4)$$

Here N_{fo} is a reference number of cycles to failure, σ_a is the fatigue strength at the reference number, k is the strength factor, and a and b are numerical constants. Since the fatigue fracture does not take place at cycles larger than 10^7 , as is shown by arrows in Fig. 5, the value of N_{fo} is set to be 10^7 . The fatigue limit defined by σ_{ao} is evaluated to be 597 MPa, 745 MPa and 796 MPa at room temperature, 473 K and 673 K, respectively. In Fig. 6, the abscissa of Fig. 5 is converted into the time to failure t_f and the extrapolation to low cycle fatigue region is conducted by using Eq. (4). The σ_a - t_f curves of

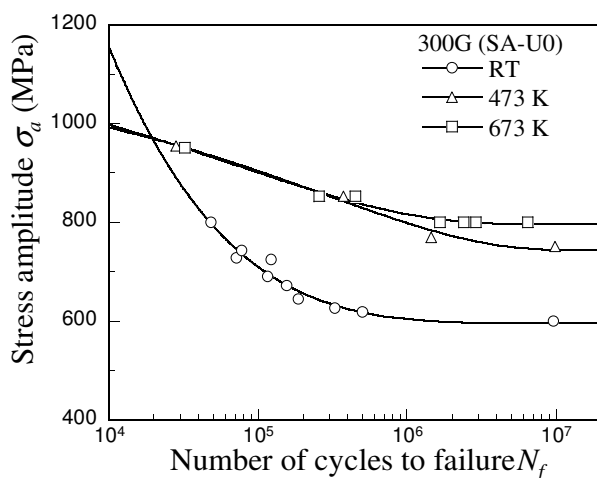


Fig. 5. SN curves of 300G steel tested at room temperature, 473 K and 673 K.

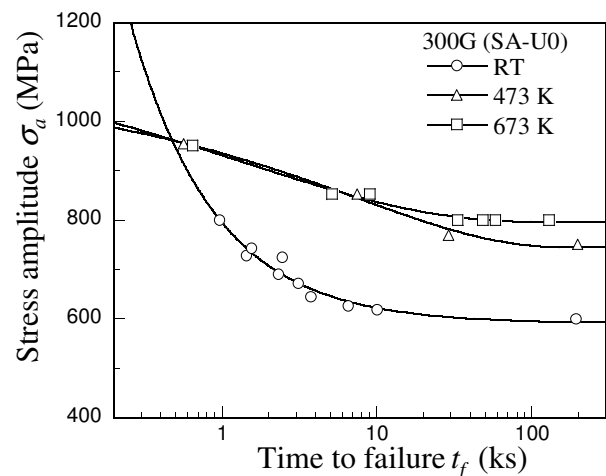


Fig. 6. Relation of stress amplitude with time to failure in 300G steel.

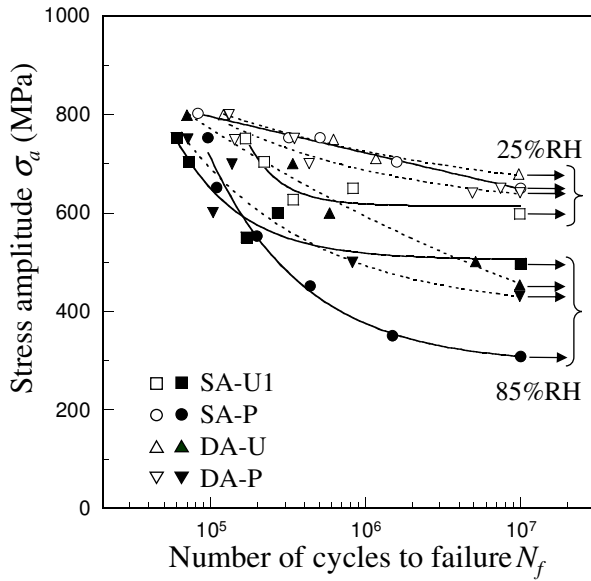


Fig. 7. SN curves of 350G maraging steels in dry and humid airs.

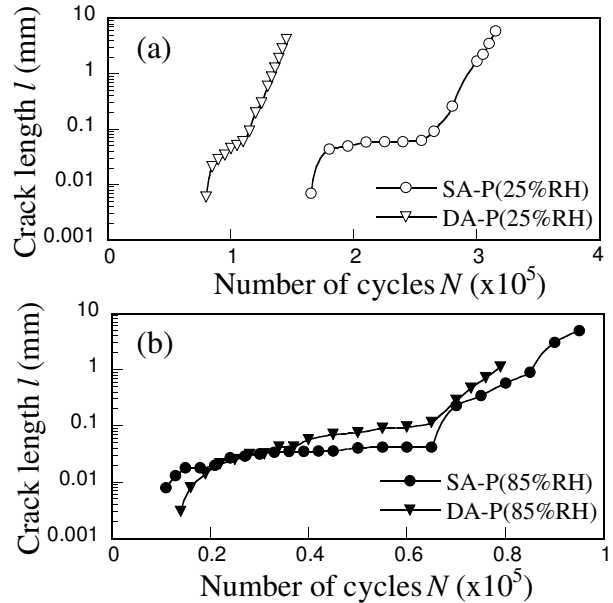


Fig. 8. Crack growth (a) in dry air and (b) in humid air.

473 K and 673 K intersect with that of room temperature at 0.4 ks ($N_f \approx 2 \times 10^4$), and the dynamic aging becomes prominent at longer time than this. It also predicts that low cycle fatigue region at shorter time than 0.4 ks shows normal temperature-dependence in which the fatigue strength is lowered by increasing temperature. One can see from Fig. 3 that static aging at 673 K already appears at shorter time than 0.4 ks. However there is no increase in hardness within 2 ks when the second-step-aging is conducted at 473 K, while dynamic aging resulting in the same increase of fatigue strength as that of 673 K starts in much shorter time. These results suggest that the microstructural change at 473 K and 673 K is enhanced with the motion of dislocations during fatigue tests. From the analysis of static aging described in the previous section, it is believed that solute atoms segregate at dislocations and impede their motion. Almost the same increase of stress amplitude at 473 K and 673 K suggests that the atmosphere of solute atoms around dislocations is saturated so quickly as to have the same suppression effect on the motion of dislocations. However, the enrichment of solute atoms may lead to the formation of dense or large precipitates at 673 K for longer duration, which results in larger fatigue limit than that of 473 K as the stress level is lowered.

3.4 Effect of two-step-aging on environmentally assisted fatigue cracking

Fig. 7 shows the SN curves of one-step-aged and two-step-aged 350G maraging steel specimens which were tested in the air of 25% RH (dry) and 85% RH (humid) at room temperature [7]. In the dry air, the one-step-aged specimens show larger fracture strength in peak-aging than in under-aging, while fatigue strength is not affected by two-step-aging. Fatigue tests in the humid air, however, result in a marked decrease in fatigue strength, especially at high cycle fatigue region. The one-step-aged specimens exhibit the increase in the susceptibility to the humid air as the aging time increases from under-aging (SA-U1) to peak-aging (SA-P). As a result, the peak-aged specimens showed the lowest fatigue strength. The addition of second-step-aging at 673 K to the SA-P specimens increases the fatigue strength significantly compared to the original value of SA-P specimens.

Cracks are initiated at very small number of cycles in the humid air compared to in the dry air, as demonstrated by Fig. 8. After the initiation stage, cracks grow steadily in both conditions, but the crack growth is accelerated in the humid air. In particular, abrupt crack propagation seems to occur

in SA-P specimen tested in the humid air (Fig. 8(b)), while such abrupt growth does not appear in DA-P specimen. This result suggests that the second-step-aging suppresses the occurrence of abrupt crack growth in the humid air, which may lead to the larger resistance to fatigue cracking than is observed in SA-P specimen (Fig. 7).

3.5 Microstructures

Fig. 9 shows the TEM images of microstructures in DA-U specimen. It is obvious from the bright field image that there are two types of precipitates having rod and spherical shapes, which are homogeneously distributed in grains. The analysis of diffraction patterns show that the rod-shaped particles are Ni_3Ti , as is shown by the dark field image (Fig. 9(b)). The fine particles of spherical shape have much larger density than that of rod-shaped $\text{Ni}_3(\text{Ti}, \text{Mo})$ particles. These features are common to the specimen one-step-aged to peak-hardening stage (SA-P) and the specimens two-step-aged at 673 K (DA series). The size and number of Ni_3Ti particles do not seem to differ significantly between these specimens.

The electrolyte extraction technique revealed that all of the specimens except SA-U1 specimen contained the particles of Ni_3Ti , Ni_3Mo , Ni_3Al , FeMo and Fe_2Mo [15]. In particular, the fractions of Ni_3Ti , Ni_3Mo and FeMo are much larger than that of Fe_2Mo . However, the contents of these phases were much less in SA-U1 specimen. This suggests that the under-aging state of SA-U1 specimen contains much more solute atoms or finer precipitates of which content cannot be measured by the electrolyte extraction technique. Over-aging at 753 K in one-step-aging led to a drastic decrease in FeMo content and a marked increase in Fe_2Mo instead, though the fractions of $\text{Ni}_3(\text{Ti}, \text{Mo})$ particles increase very slightly. Thus it is suspected that FeMo particles dissolve and more stable Fe_2Mo particles are formed at longer duration. On the other hand, no significant change was observed in the nature and contents of precipitates between SA-P and DA-P specimens. The similarity in the nature and contents of precipitates was also observed in DA-O specimen and the two-step-aged specimen in which the second-step-aging was conducted at 473 K. These results suggest that the static and dynamic hardening due to the second -step-aging at 473 K and 673 K are caused by very fine microstructures which are not identified by TEM observation and electrolyte extraction technique.

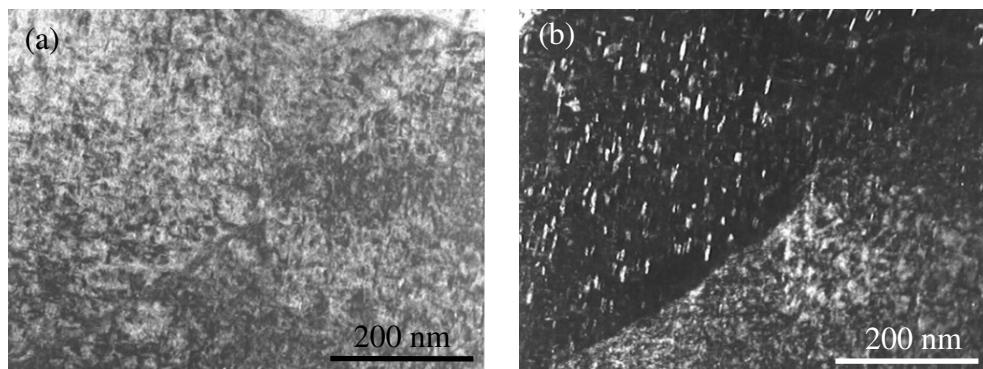


Fig. 9. Microstructures in 350G steel two-step-aged to under-aging state (DA-U) .
(a) Bright field image and (b) dark field image.

4. Discussion

The present results clearly indicate that the hardness of one-step-aged maraging steels is increased by the addition of static aging at 473 K and 673 K. The rapid increase in fatigue strength within the duration of 0.4 ks at these temperatures also suggests that the microstructural change is promoted by the motion of dislocations. As mentioned in section 3.2, both of the static and dynamic agings are

considered to be related with the precipitation which occurs via the pipe diffusion of substitutional solute atoms. In this case it is considered that the segregation of the solute atoms at dislocations precedes the precipitation at the initial stage of aging. It is well known that the misfit parameters of solute atoms in atomic size and modulus determine the magnitude of the elastic interaction of the solute atoms with dislocations. The analysis of the hardness data of ferrous alloys measured by Stephans and Witzke [16] indicate that Mo atoms have the second largest interaction with dislocations, which is comparable to that of Ti atoms [15]. From the thermodynamical viewpoint, the degree of supersaturation of solute atoms is another significant factor which enhances the segregation at dislocations. According to the phase diagrams of Fe-Mo alloy [17] and Fe-Ti alloy [18], the solubility of Ti and Mo decreases rapidly as the temperature is lowered below 773 K. It is expected that more excess Mo atoms are present during the second-step-aging or the fatigue tests at 473 K and 673 K than Ti atoms, since the content of Mo is much larger than that of Ti in the maraging steels used here. Thus such excess Mo atoms play a predominant role in interacting with dislocations at these temperatures. One can see from Fig. 3 that under-aging state accelerates the increase in hardness due to the following second-step-aging. Since the degree of supersaturation of solute atoms is expected to be larger in the under-aging state, the driving force for the segregation increases.

According to Nitta *et al.* [19] the coefficient of lattice diffusion of Mo in Fe is given by $D_{Mo} = 0.0148 \exp(-282.6 \text{ kJ/mol}/RT) \text{ m}^2/\text{s}$. The diffusion coefficient at 473 K is too small to explain the static and dynamic agings observed at this temperature. The present results rather indicate that the pipe diffusion of solute atoms is attributable to the static aging, as mentioned in section 3.2. It is considered that Mo atoms very close to dislocations migrate to the dislocations with the assistance of their elastic interaction and then diffuse along the dislocations. The stress-induced migration followed by pipe diffusion may serve effectively at 473 K. Thus the evaluated values of Q_d are considered to involve the contribution of stress-induced diffusion of solute atoms close to dislocations. Recently Christien *et al.* [20] have shown by using neutron diffraction that the dislocation density of $4 \times 10^{15} /\text{m}^2$ are generated during martensitic transformation of 17-4PH steel and it is kept nearly constant with increasing aging temperature up to 773 K. The dislocation density measured by them agrees well with $7 \times 10^{15} /\text{m}^2$ in Fe-18mass%Ni evaluated by Nakashima *et al.* [3]. Nakashima *et al.* also reported that the dislocation density was lowered to $4 \times 10^{15} /\text{m}^2$ by plastic deformation. Assuming that these results are applicable to the maraging steels investigated here, the mean spacing of dislocations becomes about 16 nm and the stress level between dislocations is 1 GPa. It is therefore considered that such high dislocation density enables the stress-induced and pipe diffusions of solute atoms to operate effectively at low temperatures.

The present results clearly show that hardness is a good measure to get insight into the microstructural change with aging time or testing temperature. Viswanathan *et al.* [21] measured the Rockwell hardness (H_{RC}) of 350G maraging steel aged at temperatures from 673 K to 823 K for various time. In order to compare their result with the present Vickers hardness data, the Rockwell hardness measured by Viswanathan *et al.* is converted into the Vickers hardness in GPa by using the hardness conversion table for steels given in ASTM E140-7. Fig. 10 shows the aging time-temperature-hardness (TTH) diagram deduced from the converted Vickers hardness data. The TTH curves have a nose-shape which is oriented toward higher temperature at shorter time. This indicates the general tendency of aging in which the nucleation and growth of precipitates proceed from the supersaturation of solute atoms to the peak aging and then decomposition and coarsening take place. It should be noted that the hardness increases to its maximum value at 673 K and 1000 ks, as the temperature is lowered. Tewari *et al.* [22] proposed a time-temperature-transformation (TTT) diagram for 350G maraging steel which is shown by broken curves in Fig. 11. The TTT curves proposed by them are conceptual ones and do not present exact profiles. The overlapping of the TTT curves on the TTH contours, however, provides a general trend pertinent to the dependence of hardness on microstructure at temperatures of 673 K ~ 823 K over a wide range of aging time.

The TTT diagram suggests that, at 753 K used as one-step-aging temperature in the present study, $\text{Ni}_3(\text{Ti, Mo})$ particles precipitates first and these particles grow accompanying the formation of fine Fe_2Mo particles which leads to the peak hardening. Our microstructural investigation, rather, indicates that $\text{Ni}_3(\text{Ti, Mo})$ and FeMo particles with much larger contents than that of Fe_2Mo are attributable to the peak hardening at 753 K. Tewari *et al.* reported that S phase was initially formed at 673 K, which was followed by the precipitation of ω phase in 10 ks. Sha *et al.* [23] found ω phase ($\text{Ni}_{47}\text{Fe}_{12}\text{Co}_1\text{Mo}_{40}$) in Fe-Ni-Mo-Co model alloy aged at 687 K for 57 ks by using APFIM. They also showed that Fe_7Mo_6 particles were formed at this aging condition. According to these results, very fine particles of S phase, ω phase and Fe_7Mo_6 are considered to play a major role in the slow hardening at 673 K.

The low-temperature boundaries of TTH curves suggests the possibility that age-hardening continues as the temperature is lowered below 673 K, and it requires longer time with the decrease in temperature. The extrapolation of the boundaries to 473 K, however, does not predict the hardness observed at this temperature. It is rather considered that the solute atoms absorbed at dislocations migrate along them to agglomerate as very fine clusters as the aging time is increased, as shown schematically in Fig. 11. Dissimilar to the aging at 673 K where lattice diffusion may also contribute to the growth of precipitates for prolonged duration, the transition from such clusters to precipitates is considerably retarded at 473 K. In fatigue tests at 473 K, however, dislocations encounter excess solutes atoms during their motion. This leads to the quick formation of solute atmosphere around the dislocation, which in turn impedes the dislocation motion and increases the resistance to fatigue cracking.

It has not been made clear why the second-step-aging improves the fatigue strength in humid air. The specimens tested in 85%RH air showed that cleavage-like facets in several grains were formed at the initiation of cracks and the cracks propagated along lath boundaries, irrespectively of the aging conditions. On the other hand, the crack initiation in 25%RH air was associated with slip in grains, followed by the crack propagation along lath boundaries. These fractographic features obtained in the previous study [24] do not provide the information on the effects of second-step-aging on fatigue cracking. The present results, however, suggest that the increase in fatigue strength in humid air is also closely related with the microstructures formed by the second-step-aging.

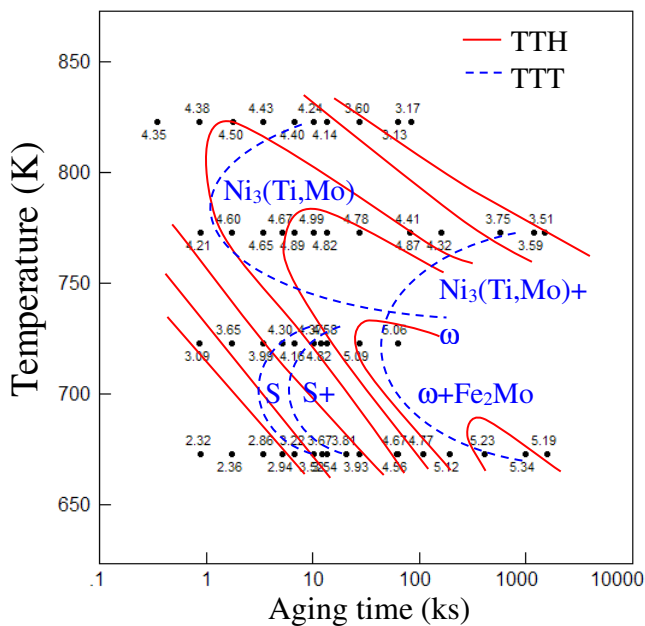


Fig. 10. TTH and TTT diagrams deduced from [21] and [22].

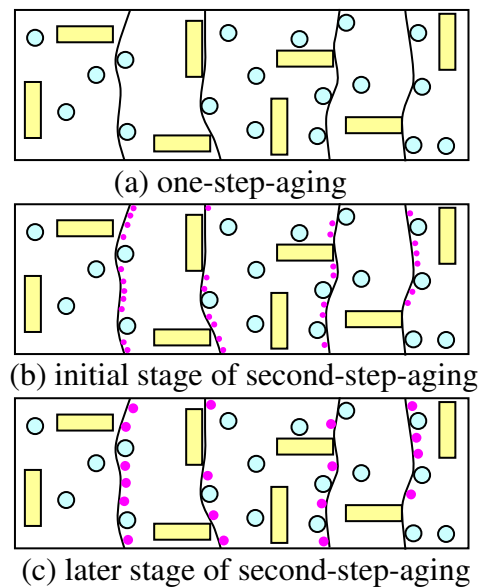


Fig. 11. Segregation and precipitation process during second-step-aging.

5. Summary

In the present study, the effects of the artificial second-step-aging prior to deformation as well as the effects of dynamical aging during deformation in Fe-18Ni maraging steels (300 and 350 grades) were investigated. The analysis of the increase in hardness with aging time in the second-step-aging at 473 K and 673 K showed that the activation energy of second-step-aging is 113 kJ/mol for initially under-aged 300G steel and 82.9 kJ/mol for initially peak-aged 350G steel. This activation energy corresponds to that of the pipe diffusion of solute atoms along dislocations. The solute atmosphere is considered to form around dislocations via the pipe diffusion and impede the motion of dislocations. Particularly the dynamic aging process takes place in the fatigue tests at 473 K and 673 K, of which effect is nearly the same. This also indicates that the fast diffusion of solute atoms to mobile dislocations causes the dynamic aging which improves the fatigue strength markedly. The microstructural observations do not provide clear evidence that new precipitates are formed during the second-step-aging. This fact also is indirect evidence that the evolution of solute atmosphere, very fine clusters or precipitates invisible in TEM are responsible for the hardening during the static and dynamic aging. The improvement in fatigue strength in humid air by the second-step-aging may be correlated closely with the microstructural change and hardening mechanism mentioned above.

References

- [1] W. Sha, Z. Guo, Maraging Steel, Modelling of Microstructure, Properties and Applications, Woodhead Publishing Limited, Oxford, 2009.
- [2] W.C. Leslie, The Physical Metallurgy of Steels, McGraw-Hill, New York, 1981.
- [3] K. Nakashima, Y. Fujimura, H. Matsubayashi, T. Tsuchiyama, S. Takaki, Tetsu-to-Hagane, 93 (2007) 459–465.
- [4] N.E. Frost, K.J. Marsh, L.P. Pook, Metal Fatigue, Dover, New York, 1999.
- [5] N. Kawagoishi, T. Nagano, M. Moriyama, Y. Ohzono, T. Ura, Trans JSME A, 71 (2005) 14–20.
- [6] N. Kawagoishi, M. Miyazono, T. Nagano, M. Moriyama, J-JSMS, 58, (2009) 787–792.
- [7] N. Kawagoishi, K. Hayashi, T. Nagano, Y. Nakamura, M. Moriyama, Y. Maeda, J-JSMS, 61 (2012) 787–794.
- [8] N. Kawagoishi, T. Iwamoto, T. Nagano, K. Morino, J-JSMS, 58 (2009) 781–786.
- [9] D. Tabor, The Hardness of Metals, Oxford Press, Oxford, 1951.
- [10] K.L. Johnson, Contact Mechanics, Cambridge University Press, Cambridge, 1985.
- [11] J.W. Christian, The Theory of Transformations in Metals and Alloys, Part I, 2nd Edition, Pergamon Press, Oxford, 1975.
- [12] V. Gerold, Precipitation Hardening, in F.R.N. Nabarro (Ed.), Dislocations in Solids, Vol. 4, North-Holland, Amsterdam, 1979, pp.219–260.
- [13] F.C. Larché, Nucleation and Precipitation on Dislocations, in: *ibid.*, pp. 135–153.
- [14] L.J. Cuddy, W.G. Leslie, Acta Met, 20 (1972) 1157–1167.
- [15] Y. Nakamura, N. Kawagoishi, unpublished.
- [16] J.R. Stephens, W.R. Witzke, J Less Common Metals, 48 (1976) 285–308.
- [17] A.F. Guillermet, Calphad, 6 (1982) 127–140.
- [18] K.C. Hari Kumar, P. Wollants, L. Delaey, Calphad, 18 (1994) 223–234.
- [19] H. Nitta, T. Yamamoto, R. Kanno, K. Takasawa, T. Iida, Y. Yamazaki, S. Ogu, Y. Iijima, Acta Mater, 50 (2002) 4117–4125.
- [20] F. Christien, M.T.F. Telling, K.S. Knight, Scripta Mater, to be published.
- [21] U.K. Vsiwanathan, G.K. Dey, M.K. Asundi, Met Trans A, 24 (1993) 2429–2442.
- [22] R. Tewari, S. Mazumder, I.S. Batrai, G.K. Dey, S. Banerjee, Acta Mater, 48 (2000) 1187–1200.
- [23] W. Sha, G.D.W. Smith, A. Cerezo, Surface Science, 266 (1992) 378–384.
- [24] N. Kawagoishi, K. Kariya, T. Nagano, M. Moriyama, Y. Nakamura, Y. Maeda, Proc 31st Symp on Fatigue, JSMS, 2012, pp.119–123.